Hydrogen Trapping in Palladium Nanoparticles Revealed by Electrochemical, X-ray Scattering, and Spectrometric Measurements

Arnaud Viola, Raphaël Chattot, Vincent Martin, Galina Tsirlina, Jaysen Nelayah, Jakub Drnec, Frédéric Maillard

▶ **To cite this version:**

Arnaud Viola, Raphaël Chattot, Vincent Martin, Galina Tsirlina, Jaysen Nelayah, et al.. Hydrogen Trapping in Palladium Nanoparticles Revealed by Electrochemical, X-ray Scattering, and Spectrometric Measurements. Journal of Physical Chemistry C, 2023, 127 (36), pp.17761-17769. 10.1021/acs.jpcc.3c04464 . hal-04223367

HAL Id: hal-04223367
https://hal.science/hal-04223367v1

Submitted on 13 Oct 2023

HAL is a multi-disciplinary open access archive for the deposit and dissemination of scientific research documents, whether they are published or not. The documents may come from teaching and research institutions in France or abroad, or from public or private research centers.

L'archive ouverte pluridisciplinaire **HAL**, est destinée au dépôt et à la diffusion de documents scientifiques de niveau recherche, publiés ou non, émanant des établissements d'enseignement et de recherche français ou étrangers, des laboratoires publics ou privés.

Hydrogen Trapping in Palladium Nanoparticles Revealed by Electrochemical, X-Ray Scattering, and Spectrometric Measurements

*Arnaud Viola [1], Raphaël Chattot [2], Vincent Martin [1], Galina Tsirlina [1], Jaysen Nelayah [3], Jakub Drnec [4], Frédéric Maillard [1, *]*

[1] Univ. Grenoble Alpes, Univ. Savoie Mont Blanc, CNRS, Grenoble INP⊥, LEPMI, 38000 Grenoble, France. ⊥Institute of Engineering and Management Univ. Grenoble Alpes

[2] ICGM, Univ. Montpellier, CNRS, ENSCM, 34095 Montpellier Cedex 5, France

[3] Université Paris Cité, CNRS, Laboratoire Matériaux et Phénomènes Quantiques 10 rue Alice Domon et Léonie Duquet, 75013 Paris, France

[4] ESRF, The European Synchrotron, 71 Avenue des Martyrs, CS40220, 38043 Grenoble Cedex 9, France

KEYWORDS: palladium nanoparticles ; hydrogen trapping ; hydrogen absorption ; hydrogen embrittlement ; wide-angle X-ray scattering.

ABSTRACT

Palladium hydrides (PdH_x) present a model system of both fundamental and applied importance: solute-induced phase transition affects evolution and electrooxidation of molecular hydrogen in water electrolysers and fuel cells respectively, as well as hydrogen storage, its sensing and catalysis of many hydrogenation reactions. It is well-documented that hydrogen (H) atoms get progressively trapped in Pd under various sorption-desorption modes, leading to embrittlement and influencing its bulk and interfacial properties. However, the intensity and progressiveness of this phenomenon remain little explored. Herein, by combining *in situ* X-ray scattering and electrochemistry, we provide evidence of continuous expansion of the lattice of 3.6 nm carbon-supported Pd nanoparticles during repeated H insertion/de-insertion cycles, resulting in a progressive loss of their reversible H sorption capacity.

INTRODUCTION

Due to the unique ability of palladium (Pd) to reversibly insert (absorb) and de-insert (desorb) large quantities of hydrogen (H) at room temperature and low pressure, the palladium-hydrogen (Pd-H) system has been widely studied. This unique property makes Pd and its alloys attractive materials for several applications including hydrogen storage [1], separation and purification [2,3], sensing [4,5] and (electro)catalysis [6,7]. H atoms can be inserted into Pd by applying a H_2 pressure. The α phase (PdH_x-α), corresponding to a PdH_x solid solution with slightly expanded lattice constant, first forms at low H_2 pressure (< 0.01 atm). The β phase (PdH_x-β), corresponding to a non-stoichiometric Pd hydride phase where H atoms occupy the octahedral lattice sites (forming a NaCl structure), forms at higher H_2 pressure. H atoms can also be inserted into Pd electrochemically, as the electrode potential (equivalent of the pressure in electrochemistry) is a measure of effective H_2 fugacity under equilibrium conditions. Similar to what was found in the gas phase, in electrochemistry, H is first dissolved in the α phase followed by formation of the β phase, and the two phases were shown to coexist in bulk Pd for intermediate values of x [8]. At room temperature and under equilibrium, the phase transition occurs at potentials of *ca*. 55-60 mV in reversible hydrogen electrode (RHE) scale.

In situ techniques [9–11] have been frequently used to provide information concerning lattice expansion/contraction of the Pd-H system. It is well documented that H insertion and formation of β hydrides cause linear expansion of the Pd lattice, adversely affecting the stability of bulk Pd samples (foils, wires, thin films), a phenomenon that is known at the macroscopic level as H embrittlement. The Pd lattice irreversibly expands upon repeated H insertion/de-insertion cycles [12], resulting in the formation of microstructural defects, such as dislocations [13,14], and modifying the rate of α↔β phase transitions [14–16]. Cycling also fragilizes the texture (distribution of

crystallographic orientations) [17] and changes the dimensions (length and thickness) [18] of bulk Pd materials while irreversible cracks and delamination were reported for Pd thin film samples [11,19]. The behavior of Pd nanocrystallites differs. Lee *et al.* first reported that irreversible mechanical deformation of Pd films is suppressed in the films thinner than 20 nm [19]. Moreover, if dislocations easily appear in bulk Pd materials, they are unlikely to form in Pd nanoparticles (NPs) smaller than 300 nm, as recently shown by Uvelstad *et al.* [13]. According to Vogel *et al.* [20], H can be reversibly inserted/de-inserted in/from 4 to 6 nm Pd NPs with no modification of the crystal structure. On the contrary, non-closing pressure-composition-isotherm curves and more expanded lattice constant after H de-insertion have been frequently reported for Pd nanomaterials after H insertion/de-insertion experiments [21–26]. Recently, Liu *et al.* [27] investigated H trapping into carbon-supported Pd NPs with sizes between 1.4 and 6.0 nm. They reported an increasing loss of H sorption capacity with decreasing Pd NPs size. Density functional theory (DFT) and tight-binding calculations supported the experimental findings, and revealed that H atoms are trapped in the subsurface interstitial sites. However, this study was limited to a single sorption-desorption cycle in the gas phase. Campesi *et al.* [28] observed that the total H sorption capacity of 2 nm Pd clusters/porous carbon composite at 5 atm H_2 markedly decreases after the first insertion/de-insertion cycle and in a less pronounced manner later on, yielding H:Pd atomic ratios of 0.78, 0.55 and 0.49 for the first, second and third cycles, respectively. Using unsupported Pd NPs as a catalyst for ammonia-borane hydrolysis, Jose *et al.* [23] reported that some H atoms remain trapped in the Pd lattice even after the reaction, leading to expanded Pd lattice constant, more pronounced after 10 cycles than after the first one. In contrast, Rather *et al.* [29] reported stable H storage capacities (measured at 25°C and 1.7 MPa H_2 pressure) for *ca.* 13 and 8 nm Pd NPs after up to 8 H insertion/de-insertion cycles.

Importantly, the samples were outgassed under vacuum at 200°C between successive cycles, which may account for the apparent stability of their H sorption capacity.

With the motivation of providing comprehensive evidence of H trapping process in Pd NPs and of clarifying the influence of this process on their long-term H sorption capacity, we combined here *in situ* wide-angle X-ray scattering (WAXS), *in situ* inductively-coupled plasma mass spectrometry (ICP-MS), identical-location transmission electron microscopy (IL-TEM) and coulometric quantification of the amount of H inserted and de-inserted in/from Pd NPs. The results show continuous expansion of the Pd lattice during repeated H insertion/de-insertion cycles, resulting in a progressive loss of their reversible H sorption capacity and in appearance of delay in lattice relaxation during H de-insertion.

METHODS

Details about materials, methods, and experimental techniques are presented in Supplementary Information.

RESULTS & DISCUSSION

Figure 1a shows characteristic low- and medium-magnification transmission electron microscopy (TEM) images of the commercial carbon-supported Pd catalyst (Pd/C) used in this study. The Pd NPs are isolated and homogeneously distributed onto the Vulcan XC72 support. Their number-averaged mean NP size is $\overline{d_n} = 3.6 \pm 0.7\ nm$ (see **Figure S1** in **Supporting Information** for more details). The Pd content amounts to 17.6 wt.%, as determined by microwave-assisted digestion of a given mass of catalyst in aqua regia, dilution and analysis by ICP-MS. **Figure 1b** displays a typical cyclic voltammogram (CV) of the Pd/C sample recorded between 0.0 and 0.6 V

in Ar-saturated 0.1 M $HClO_4$ (Note that all electrode potentials are referred to the reversible hydrogen electrode, RHE). In agreement with literature, peaks 1 and 1' can be ascribed completely or partly to the adsorption and desorption of underpotentially-deposited H, and peaks 2 and 2' to the insertion (absorption)/de-insertion (desorption) of H mostly into/from the PdHx-β phase [30]. The PdHx-α phase contribution can be distributed between these two features. For lower potentials, the formation of molecular H_2 (dissolved in solution) proceeds simultaneously to the insertion of H ("tail" 3).

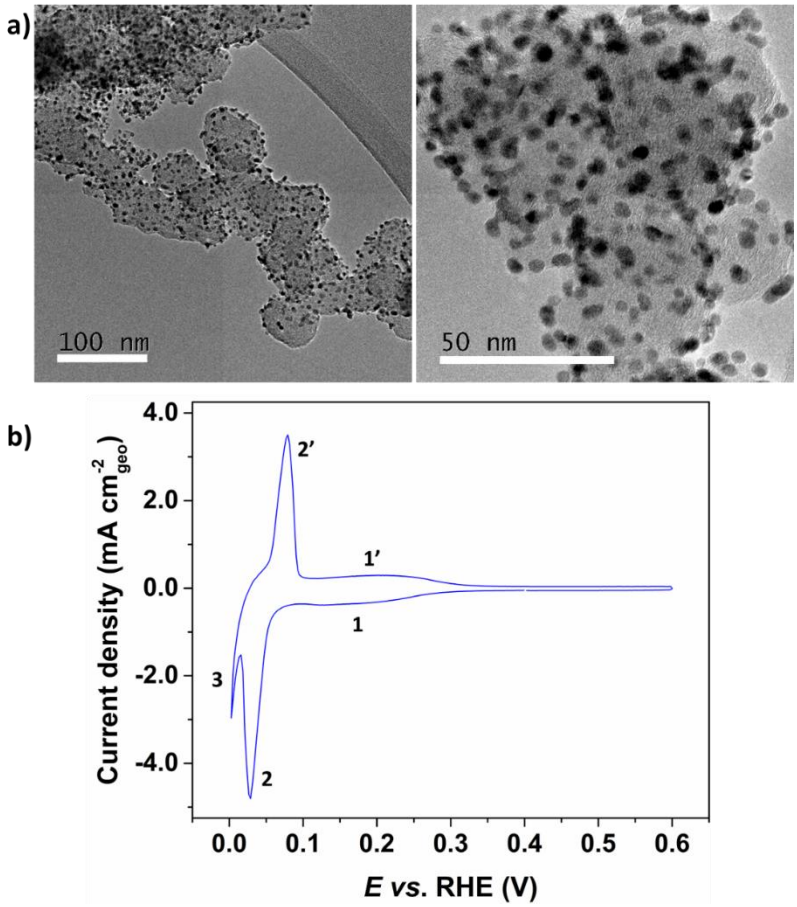

Figure 1. **Microscopic and electrochemical characterization of the Pd/C nanocatalyst used in this study.** a) Low- and medium-magnification conventional TEM images, and b) cyclic voltammograms recorded on the Pd/C catalyst in Ar-saturated 0.1 M $HClO_4$ at a potential sweep

rate of 10 mV s^{-1} (starting from 0.4 V by a cathodic scan). The measurements were performed using a Pd loading of 30 μg_{Pd} cm^{-2}_{geo} and a temperature of 25 °C.

To track the changes in structure of the Pd/C NPs during the H insertion/de-insertion process, we performed *in situ* WAXS experiments at the European Radiation Synchrotron Facility (ESRF, Grenoble) using a home-made electrochemical flow cell, previously introduced in reference [10]. A WAXS pattern measured at E = 0.40 V in Ar-saturated 0.1 M $HClO_4$ is represented in **Figure 2a**. It displays the expected reflections for the face-centered cubic structure of Pd. The Pd lattice parameter obtained from Rietveld refinement analysis of the WAXS pattern was 3.8945 Å, matching with reported values for Pd films of 3.892 Å and ~3.897 Å obtained by Benck *et al.* [11] and Lander *et al.* [9], respectively. This value slightly exceeds 3.889 Å found recently for the same catalyst after cycling in alkaline solution [10], and also the values for Pd powder available in the ICDD database (*e.g.*, 3.8874 and 3.8898 Å). This can result from 0.006 Å uncertainty of calibration, as discussed in **Supporting Information**.

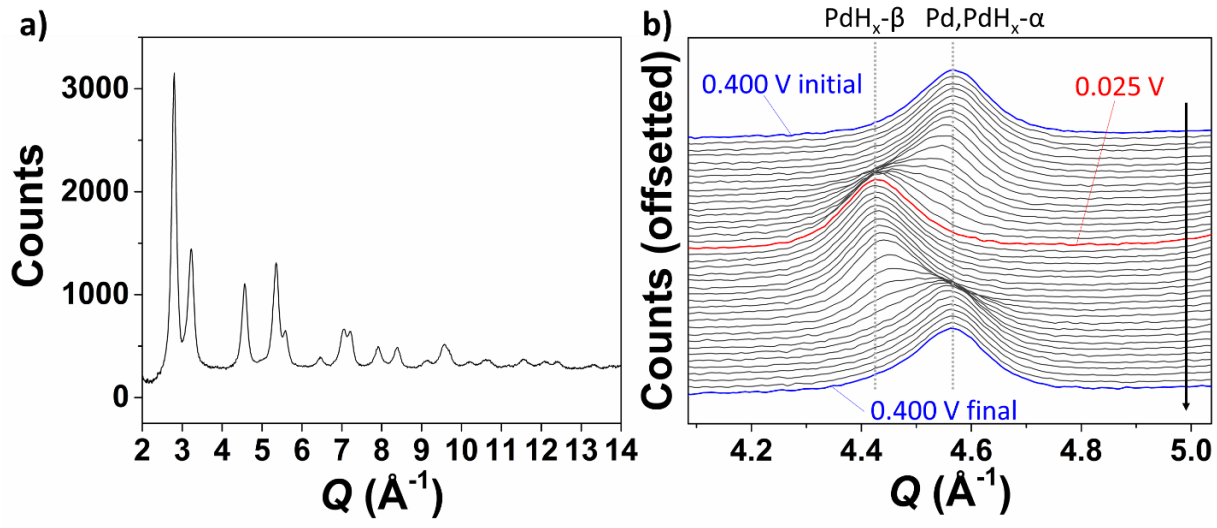

Figure 2. Time-resolved monitoring of insertion and de-insertion of H atoms into the Pd/C nanoparticles during cyclic voltammetry. a) Background subtracted WAXS pattern recorded *in*

situ on the Pd/C nanocatalyst at 0.40 V in N_2-saturated 0.1 M $HClO_4$, and b) zoom on the Pd (220) reflection during a 5 mV s^{-1} cyclic voltammogram. During the negative-going potential sweep (H insertion), the Pd (220) reflection shifts to smaller momentum transfer (Q) values and splits into two distinct reflections, signaling the PdH_x-α→β phase transition. The PdH_x-α→β phase transition is then completed, resulting in the formation of the PdH_x-β phase. The opposite behavior is observed during the positive-going potential sweep (H de-insertion).

A 5 mV s^{-1} cyclic voltammogram (CV) was then performed to sweep the electrode potential from 0.400 to 0.025 V while simultaneously recording the WAXS patterns. As seen in **Figure 2b**, during the negative-going potential sweep, the Pd (220) reflection progressively shifts to smaller Q values before splitting into two distinct reflections for $0.028 < E < 0.056$ V. Since the WAXS pattern is the convolution of the scattered X-rays from the entire population of NPs, these two reflections can be interpreted in two ways: (i) some Pd/C NPs turn into β phase at a lower overpotential than others or (ii) the α and β phases co-exist in the *ca*. 3.6 nm Pd/C NPs. The first scenario is likely to occur if the Pd/C NPs are not homogeneous in size and shape or if the electric potential is inhomogeneously distributed during the CV. Influence of the WAXS pattern by ensemble effects is very unlikely given the narrow size distribution of the Pd/C catalyst (**Figure S1**) and the quasi-absence of aggregated/agglomerated Pd nanocrystallites. Moreover, the *in situ* WAXS experiments were performed using an electron-conducting glassy carbon backing electrode, a platinum counter electrode and a concentrated liquid electrolyte to prevent ohmic drop. We thus reliably relate the two reflections to the co-existence of the α and β phases in the Pd/C sample, in line with former findings of Chattot *et al*. for the same commercial Pd/C nanocatalyst in N_2 saturated 0.1 M NaOH[10]. The WAXS patterns also show that the PdH_x-α↔β phase transition is completed at $E = 0.025$ V (corresponding pattern colored in red), resulting in the formation of

the PdH_x-β phase with a lattice parameter of 4.017 ± 0.006 Å. Sweeping back the potential to 0.400 V (corresponding pattern colored in blue) leads to the PdH_x-β→Pd,PdH_x-α phase transformation.

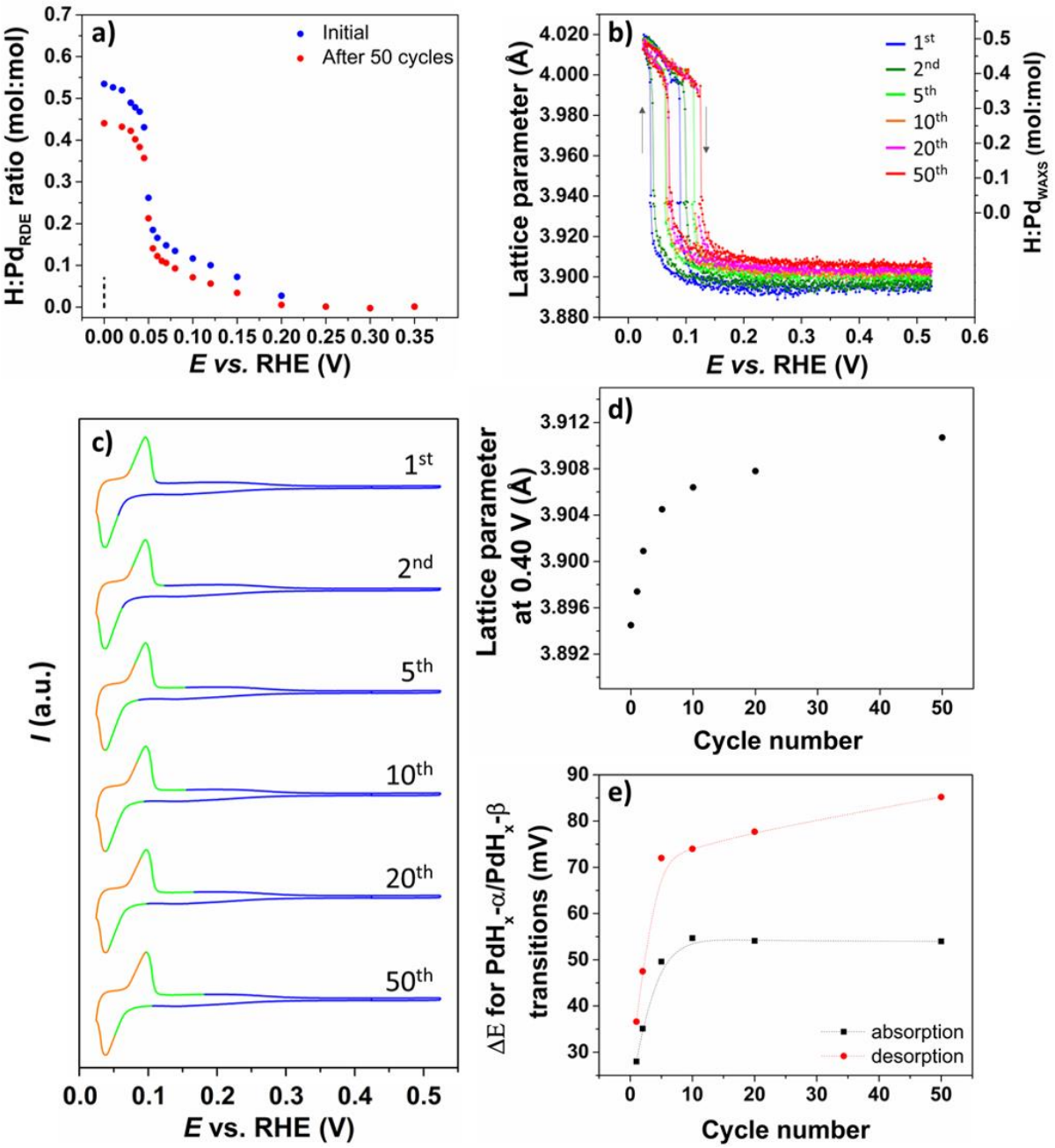

Figure 3. Monitoring the hydrogen-induced phase transformation of Pd/C nanoparticles *via* the combination of electrochemistry and *in situ* WAXS. (a) $H:Pd_{RDE}$ ratio determined by coulometric

extraction before (blue curve) and after (red curve) 50 potential cycles between 0.025 and 0.525 V in Ar-saturated 0.1 M $HClO_4$. The dashed line corresponds to the contribution of adsorbed H calculated from Q_{Cu} charge (see **Figure S2**). (b) Variation of the lattice parameter and of the H:Pd_{WAXS} ratio in the PdH_x-β phase during 50 cyclic voltammograms between 0.025 and 0.525 V in Ar-saturated 0.1 M $HClO_4$. For the sake of clarity, only the lattice parameter of the predominant (most intense) phase is plotted at a given electrode potential. The H:Pd ratio in the PdH_x-β phase is calculated using its lattice parameter and the calibration curve reported in reference 11. (c) Successive cyclic voltammograms between 0.025 and 0.525 V at 10 mV s^{-1} (all cyclic voltammograms started from 0.4 V by a cathodic scan). To illustrate which phase predominates in each potential region, the CV trace is colored in blue when only Pd, PdH_x-α is detected, in orange when only PdH_x-β is detected, and in green when the PdH_x-α and PdH_x-β phases coexist. (d) Evolution of the Pd, PdH_x-α lattice constant at 0.40 V and (e) the potential interval where Pd,PdH_x-α and PdH_x-β coexist during H insertion (in black) and H de-insertion (in red). All measurements were carried out with 30 μg_{Pd} cm^{-2} catalyst loading in N_2 or Ar-saturated 0.1 M $HClO_4$ at 25 °C.

To quantify the amount of H de-inserted from the 3.6 nm Pd/C NPs after insertion at various electrode potentials, denoted below H:Pd_{RDE} (blue curve on **Figure 3a**), we slightly modified the coulometric method introduced by Sherbo *et al.* [31]. H was first inserted into the Pd/C NPs by maintaining a given potential between 0.00 V < E < 0.40 V for 60 s. Subsequently, the potential was switched to E = 0.40 V to extract H, and the H de-insertion charge was used to calculate the H:Pd molar ratio (knowing the exact mass of Pd loaded onto the thin-film rotating disk electrode from ICP-MS measurement). More experimental details about the coulometric quantification of the Pd:H ratio can be found in the **Supporting Information**. In line with the $i(E)$ response displayed in **Figure 1b**, the insertion of H starts from *ca.* 0.1 V, then the H amount sharply

increases at *ca.* 0.05-0.07 V and reaches a pseudo-plateau at *ca.* 0.02 V. Further decreasing the electrode potential leads to an increased H:Pd ratio, which is probably overestimated since part of the electrical charge recorded at 0.40 V arises from the electrooxidation of molecular H_2 generated during the H insertion step. The H:Pd ratio measured by this coulometric method amounts to 0.53 at 0.00 V. According to the method described above, measured H:Pd ratios comprise contributions of inserted (in the Pd lattice) but also adsorbed H. The H quantity in the region preceding the α to β phase transition at potentials below *ca*. 0.06 V on **Figure 3a** can be partly assigned to adsorbed hydrogen (1 and 1' contributions in **Figure 1b**) with a certain contribution of PdH_x-α phase formation. The contribution of adsorbed H to the total H:Pd ratio was quantified by the copper underpotential deposition method (Cu UPD). Briefly, the charge for the stripping of underpotentially-deposited Cu monolayer (Q_{Cu}) was divided by two to obtain charge Q_{Had} corresponding to the formation of a monolayer of adsorbed H (Q_{Had} = ½ Q_{Cu}). More details and discussion about the Cu UPD method can be found in **Supporting Information**. We determined a Q_{Had} of 0.38 ± 0.03 mC, *i.e.* adsorbed H contributes to 0.07 on the H:Pd ratio, leading to a real H:Pd ratio of 0.46 at 0.00 V (see also **Figure S3** and discussion in **Supplementary information** for additional analysis of H:Pd ratios). The determined H:Pd ratio is low relative to what is generally determined on bulk Pd under equilibrium conditions, which we ascribe to the finite Pd NP size. WAXS observations nevertheless solidly establish the fact that PdH_x-β phase is formed under the *in situ* conditions used here.

To gain quantitative insights into the reversibility of the H insertion/de-insertion process, the PdH_x composition *vs*. potential was also determined after 50 CVs between 0.025 and 0.600 V at a potential sweep rate of 5 mV s^{-1}. Comparing blue and red curves in **Figure 3a**, we found a 19 % decrease of the H:Pd_{RDE} ratio at 0.025 V (H:Pd_{RDE} at 0.025 V = 0.43 ± 0.02 / 0.35 ± 0.02

before/after the 50 CV cycles, respectively), assuming that adsorbed H contribution remains the same, consistently with the continuous decrease of the coulometric charge associated with H-insertion/deinsertion in RDE set-up was observed during successive CVs (see **Figure S4**) The observed modification of the H insertion properties is accompanied by changes in the Pd,PdH_x structure as illustrated by **Figure 3b**. In particular, the value of the PdH_x-β lattice parameter measured at 0.025 V is constant (4.017 ± 0.006 Å) but increases from 3.895 Å to 3.911 Å at 0.400 V (see **Figure 3d**). This relative irreversible increase (~0.4 %) of the lattice parameter after 50 cycles agrees with the relative increase of nearest Pd-Pd distance of 0.73 % and 0.36 % reported by Liu *et al.* for 2 and 6 nm Pd particles, respectively, after a single H sorption/desorption cycle[27]. Let us also stress that Rietveld refinement analysis of the WAXS patterns measured at 0.40 V indicates that the microstrain values (**Figure S5**) increase with the number of H insertion/de-insertion cycles (from 93 to 129 %% for the Pd/C catalyst before and after 50 CVs, respectively), suggesting that strain progressively and heterogeneously develops within the Pd/C NPs during repeated H insertion/de-insertion cycles.

To gain further insights into the Pd nanostructure – H sorption capacity relationship, we compared the information provided by electrochemistry and WAXS measurements. The potential regions where the PdH_x-α or PdH_x-β lattices are individually observable or co-exist are represented in blue, orange and green, respectively in **Figure 3c**. At cathodic scans, the potential of PdH_x-β phase appearance (starting point of green segments) becomes more positive with cycle number (0.056 V and 0.106 V for the 1st and 50th cycles, respectively). Moreover, starting already from the 5th cycle, this potential corresponds to very low charge spent for H sorption. Assuming the hypothesis of accumulating trapped H, one can assign this shift to participation of both trapped and newly inserted H in PdH_x-β phase formation. The end of green segments/start of orange segments

demonstrates the same shift: lattice expansion corresponding to pure PdH_x-β phase starts earlier with cycle number (0.028 V for the 1st and 0.052 V for the 50th cycles). During the 50th cycle, it starts when less than a half of newly inserted H penetrates to the lattice, *i.e*. a lot of H undergoes sorption into already expanded Pd. At anodic scans, the appearance of two-phase region (the end of orange segments, and the start of green segments) shifts to more positive potentials. In the 1st cycle, PdH_x-α phase structural signatures appear when only a small portion of H is de-inserted (at 0.037 V), when in the 50th cycle about a half of H is de-inserted before the lattice starts to relax (at 0.085 V). Moreover, lattice relaxation in the 50th cycle corresponding to the appearance of Pd metal takes place only at *ca.* 0.20 V, and results in still extended PdH_x-α phase lattice.

The described behavior results in a pronounced widening of the potential region in which PdH_x-α and PdH_x-β phase lattices coexist (**Figure 3e**). These structural changes are pronounced initially and reach a pseudo-plateau after *ca*. 10 cycles (**Figure 3b-d-e**). The absence of correlation between the charge spent for H insertion/de-insertion and lattice expansion-relaxation events becomes more pronounced with cycling, and the loss of correlation is accompanied by the development of lattice microstrain (**Figure S5**).

The comparison between the H:Pd ratios measured/estimated from electrochemical and X-ray measurements is also enlightening. Using the linear calibration between the H:Pd ratio and the PdH_x-β lattice parameter reported by Benck *et al* .[11], the Pd lattice parameter in the PdH_x-β phase was converted into a H:Pd ratio, denoted $H:Pd_{WAXS}$. As illustrated by **Figure 3b**, the $H:Pd_{WAXS}$ ratio at 0.025 V was independent of the number of CV cycles (0.49 ± 0.035), suggesting that the same quantity of H was inserted in the Pd/C NPs at this potential. This seems to be in contradiction with the 19 % decrease of the $H:Pd_{RDE}$ ratio experimentally measured at 0.025 V (**Figure 3a**). As the $H:Pd_{RDE}$ is precisely determined by measuring the H insertion/de-insertion charge and the mass

of Pd deposited on the working electrode (ICP-MS measurement, see **Supporting Information**), while the H:Pd_{WAXS} is estimated from the variation of the PdH_x-β lattice parameter, the difference between the H:Pd_{WAXS} and H:Pd_{RDE} ratios may arise from two reasons: either the absence of correlation between lattice expansion and reversibly inserted H amount under less equilibrium conditions, or the detachment or the dissolution of Pd nanocrystallites during the 50 CVs.

To determine whether the changes in the lattice structure are accompanied by changes in size or morphology of the Pd/C nanoparticles, we used identical-location aberration-corrected (high-resolution) transmission electron microscopy (IL-(HR)TEM). Five different regions of the Pd/C sample were imaged before/after 1,000 square potential cycles between 0.400 and 0.100 V (10 s at each potential), Subsequently, 1,000 square potential cycles between 0.400 and 0.025 V were performed (**Figure 4**), followed by 1,000 square potential cycles between 0.400 and 0.000 V (see **Figure S6**). The IL-TEM images presented in **Figure 4** and **Figure S6** suggest that the Pd NPs neither change in size and morphology nor detach from the Vulcan XC72 support. Interestingly, IL-HRTEM showed slight movements of the Pd NPs after the 1,000 square potential cycles between 0.400 and 0.025 V, in qualitative agreement with former observations by Paciok *et al*. on Pt/C nanocatalysts [32]. They observed that 17 % of the Pt NPs move from their initial position during a 24 h polarization at E = -0.10 V in 0.5 M H_2SO_4. Longer polarization resulted in no further noticeable changes in their location. The results were rationalized by considering a decrease of attractive Van der Waals forces resulting from the adsorption of H onto the Pt/C NPs.

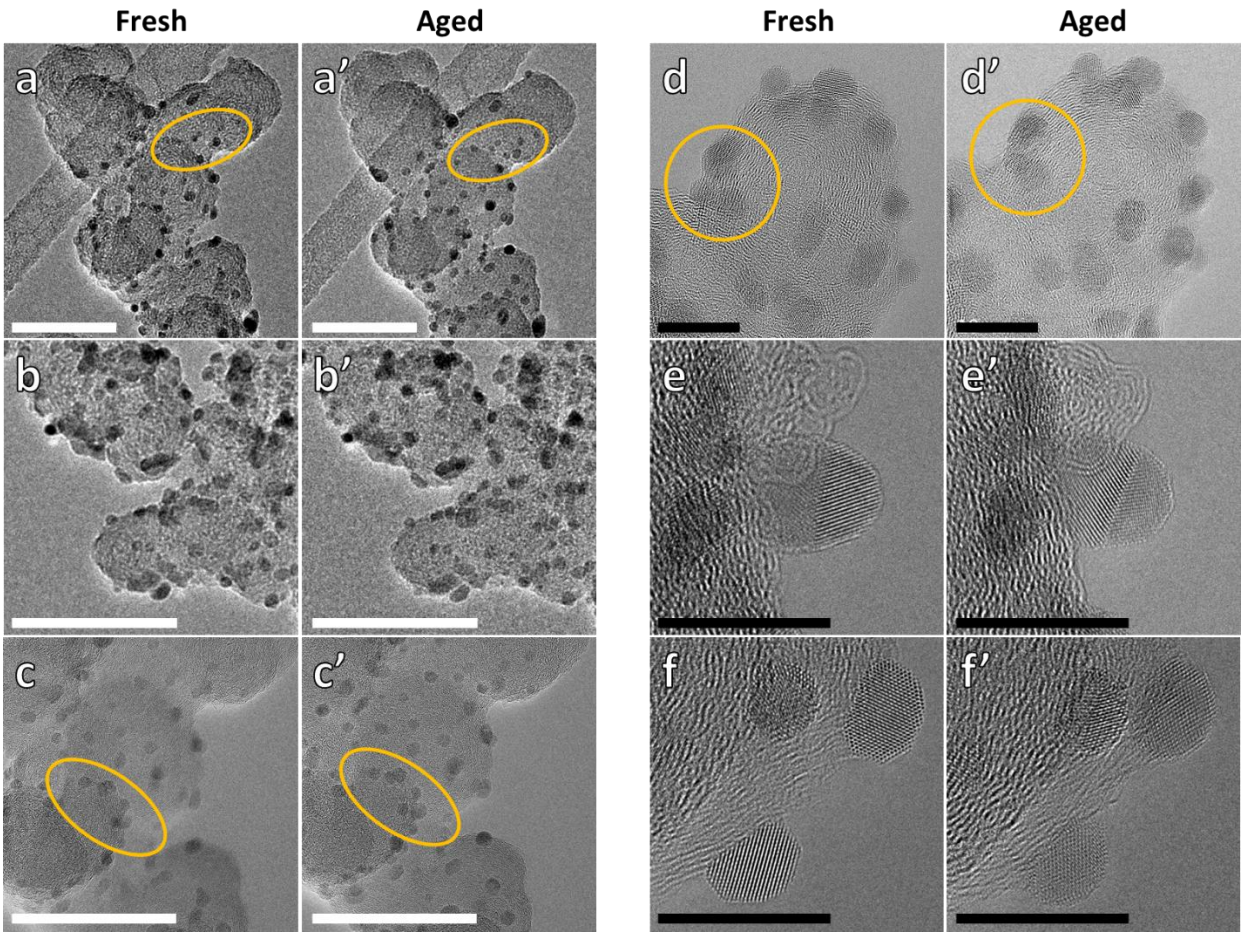

Figure 4. Identical-location aberration-corrected transmission electron microscopy images illustrating slight movements of Pd nanoparticles onto the Vulcan XC72 support during potential cycling. Aberration corrected a-b) low -magnification (x100k), c) medium-magnification (x400k) and d-f) high resolution (x800k) TEM images of 20 wt.% Pd/C, a-f) before and a'-f') after 1,000 square potential cycles between 0.025 and 0.400 V (10 s each) in Ar saturated 0.1 M $HClO_4$, T = 25°C. The yellow circles point towards slight movements of the Pd nanoparticles onto the Vulcan XC72 support. White scale bar 50 nm, black scale bar 10 nm.

To precisely estimate the amount of Pd being dissolved from the Pd/C NPs during the 50 CVs, we used an electrochemical flow cell coupled *in situ* to an ICP-MS (see Refs.[33,34] and **Supporting Information** for more details). **Figure 5** shows time- and potential-resolved Pd concentration

profiles during the break-in procedure (composed of 400 cycles between 0.100 and 0.500 V at 500 mV s^{-1}) or 25 cycles between 0.025 and 0.600 V at 5 mV s^{-1}. The *in situ* ICP-MS measurements show that the Pd concentration signal amounts to 10 ng L^{-1} maximum during the break-in procedure. The 25 cycles at 5 mV s^{-1} allow a better resolution in time and potential. The dissolution of Pd initiates during the the very beginning of the anodic potential sweep, and reaches a maximum of 10 ng L^{-1} (equivalent to about 4 ng_{Pd} $g^{-1}{}_{Pd}$) at *ca*. 0.05-0.10 V. Dissolution of Pd during H-deinsertion/desorption (positive-going potential sweeps) is a striking previously unreported result. Overall, the mass of Pd dissolved during the break-in and the subsequent 25 cycles was estimated to be inferior to 0.2 ng representing 0.003 ± 0.001 % of the total Pd mass loaded in the thin-film electrode. We can thus reliably discard any influence of the dissolution of Pd on the change in H insertion/de-insertion properties.

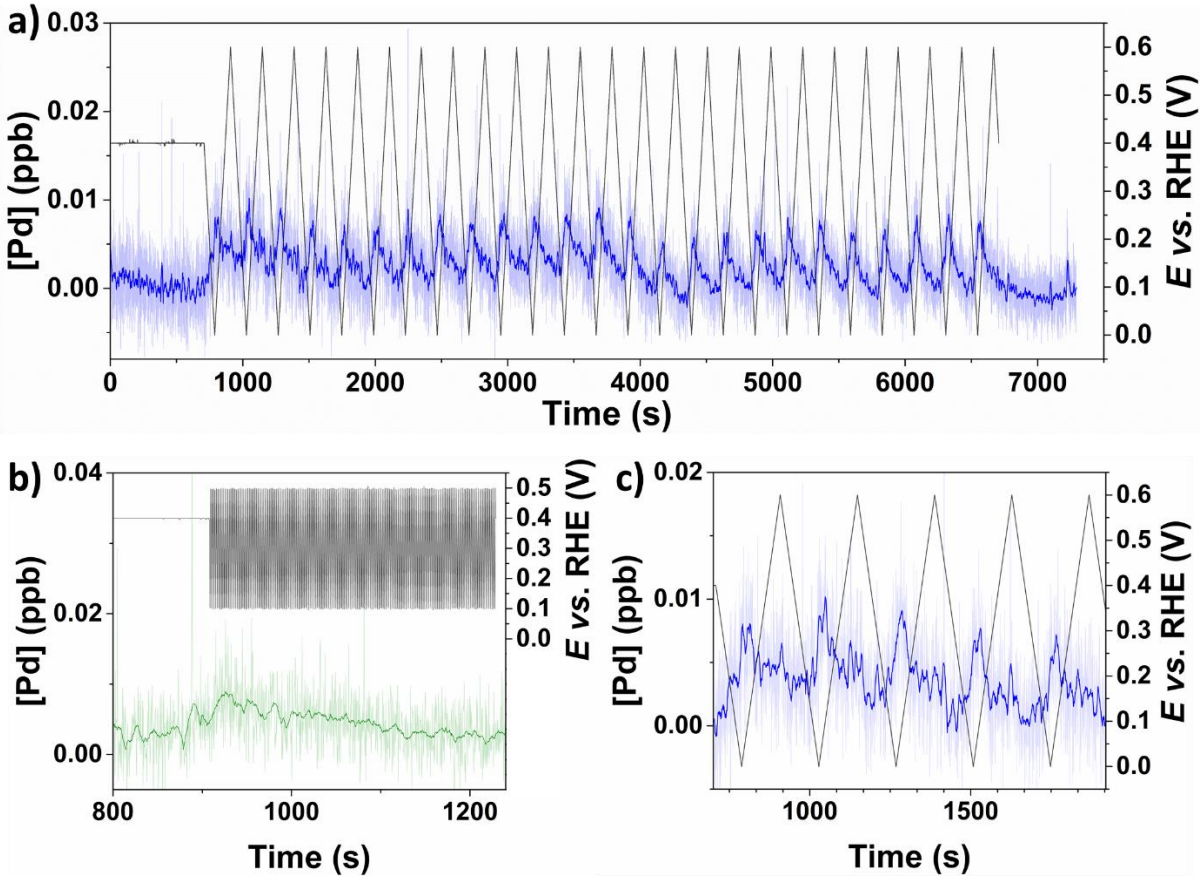

Figure 5. ***In situ*** **monitoring of the amount of Pd being dissolved during successive cyclic voltammograms**. a) corresponds to the cycles between 0.025 and 0.600 V and b) to the break-in. c) is a focus on the first five cycles. The blue and green lines are Savitzky-Golay averages (50 pts window) of the raw data points plotted with transparency for clarity. Ar-saturated 0.1 M $HClO_4$, $T = 25°C$.

Summarizing all experimental results, the lattice parameter in the PdH_x-β phase at 0.025 V remain almost constant during repeated H insertion/de-insertion cycles. Meanwhile, the value of the Pd,PdH_x-α lattice parameter at 0.400 V continuously increases. These changes in the lattice structure of the Pd/C NPs are neither accompanied by a noticeable change in their size and morphology, nor with a significant release of Pd^{2+} ions in solution but they lead to a quantitative

decrease of the reversible H:Pd_{RDE} ratio. Taken all together, the results then confirm that a fraction of H atoms remains trapped in Pd lattice at least in the timescale of our experiment, *i.e*. the rate of H insertion is essentially faster than the H de-insertion rate. This hypothesis is in line with the single-cycle results of Liu *et al.* for Pd NPs during gas phase H sorption [27]. The authors reported that smaller Pd NPs are more prone to trap H, with the loss of H sorption capacity amounting to *ca*. 26 % for 1.4 and 2 nm Pd/C NPs. In this work, the amount of trapped H atoms approaches 19 % for 3.6 nm Pd/C NPs, in quantitative agreement with the values of 26 % and 9 % reported by Liu *et al.* for 2 and 6 nm Pd/C NPs, respectively. Complementary *in situ* WAXS and electrochemical experiments revealed that (i) the Pd lattice parameter measured at E = 0.40 V after the 50 CVs remains constant for more than 5 minutes (see **Figure S7**) and that (ii) no measurable current associated to H desorption was detected after a few seconds during the coulometric H de-insertion experiment (see **Figure S3a**). We thus conclude that H de-insertion kinetics does not undergo substantial changes during the 50 CV cycles, and that the progressive increase of the PdH_x-α phase lattice parameter after the 50 consecutive cycles, the observed H trapping and the microstrain development are mutually interrelated events

Finally, to confirm that H atoms remain trapped into the Pd NPs, we also designed an additional experiment, leaning on the work of Liu *et al*. [27]. Briefly, a thin-film of Pd/C catalyst was electrochemically characterized before (fresh catalyst) and after 50 CVs between 0.025 and 0.600 V (aged catalyst). In line with what was found in **Figure 3e**, the H de-insertion charge decreased during the 50 CVs (**Figure 6a**), translating into a drop of the H:Pd_{RDE} ratio from 0.43 ± 0.02 to 0.35 ± 0.02 (**Figure 6b**). After this second characterization, the thin-film rotating disk electrode was removed from the electrochemical cell, rinsed with MQ-grade water and vacuum-pumped for 10 h at 150°C to desorb the trapped H, and a characterization CV was recorded in the

same experimental conditions as initially. The near-perfect superposition of the initial and the final CVs, and the associated increase of the quantity of de-inserted H are unequivocal evidences that H atoms were trapped in the Pd/C material during the 50 CV cycles.

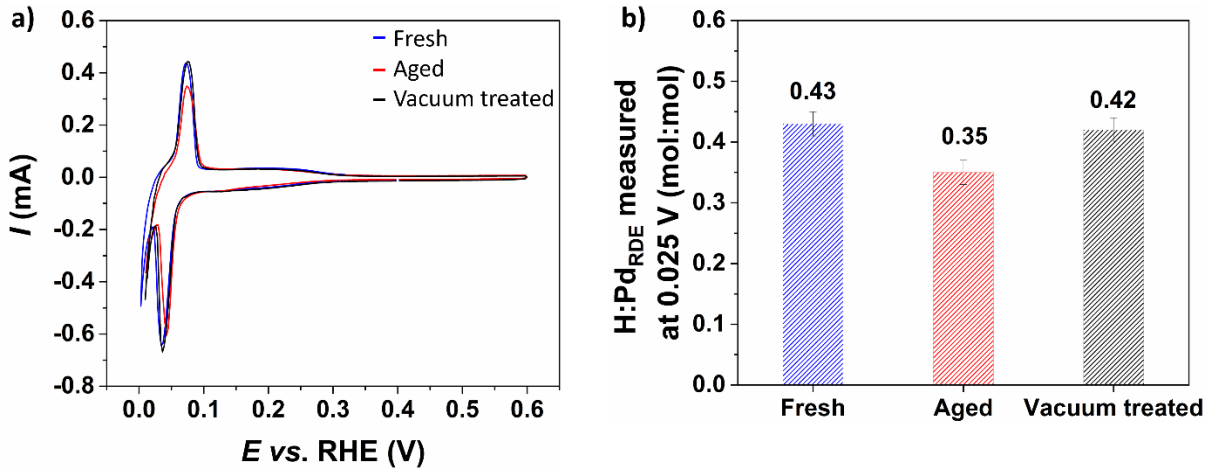

Figure 6. Electrochemical evidence of H trapping into Pd/C nanoparticles. a) Cyclic voltammograms recorded on the fresh (blue curve) and aged (red curve) Pd/C catalysts and after 10 h at 150°C under vacuum (black curve). All cyclic voltammograms started from 0.4 V by a cathodic scan and were measured at a potential sweep rate of 10 mV s^{-1}. In b), the same color codes are used to represent the $H:Pd_{RDE}$ ratio measured at 0.025 V and corrected for H adsorption. The measurements were performed in Ar-saturated 0.1 M $HClO_4$ at T = 25 °C. Rotation rate 1600 or 2500 rpm for a) and b), respectively.

The results presented in this study therefore suggest that, similarly to what was observed during catalytic reactions [23], H atoms may trap during electrochemical insertion/de-insertion at low enough RHE potentials. Let us however stress that trapping as studied in this work does not corresponds to complete equilibration of Pd-H system, first of all because of unavoidably slow phase transition [35]. In frames of the time scale available for *in situ* structural characterization, we solidly documented that lattice expansion and reversible H sorption are not completely correlated:

lattice parameter hysteresis loop is shifting to more positive potentials than corresponding charge hysteresis (compare **Figures 3b and S3**). This factor of finite characterization time appears also for H trapping analysis based on irreversible lattice expansion [27] (see additional remarks in **Supplementary Information** after **Figure S3**).

One can assume that the expansion itself provides the traps, *i.e.* new defective positions supporting stronger bonding and, correspondingly, slower de-insertion of H. This trapped H can be formally assigned to PdH_x-α phase despite its specific sorption energy, as it is stable in the lattice just at typical PdH_x-α phase pressures/potentials, and could be finally extracted under equilibrium conditions. The amount of this trapped H can be much higher as compared to PdH_x-α phase solid solution in ideal Pd lattice. Namely, H:Pd values up to ~0.06 were reported for thin Pd films[36] , and >0.03 for dispersed electrodeposited Pd [37]. Our estimate of the quantity of trapped H agrees well with these quantities. The principal aspect of our observation is generation of the traps by H inserted in subsequent cycles, in contrast to native defects typical for some Pd materials.

The results reported here are important for a fundamental understanding of structure – catalytic activity relationships on Pd-based nanomaterials. Indeed, according to the *d*-band theory pioneered by Hammer and Norskov, trapping of H atoms into the Pd lattice drastically changes its electronic states, broadening its *d*-band, and resulting in a negative shift of the *d*-band center. The latter in turn will lead to a change in the catalytic properties of Pd. For example, $PdH_{0.43}$ NPs were shown to be more active for methanol oxidation reaction compared to the pure metal Pd counterparts[38]. Schmidt *et al*. have also recently shown that expansion of the Pd lattice leads to weaker adsorption energy of adsorbed H, enhancing the hydrogen evolution reaction rate in acidic medium[39].

CONCLUSIONS

In summary, our results shed fundamental light into the loss of H sorption capacity of Pd/C nanoparticles during repeated H insertion/de-insertion cycles. By combining electrochemistry and wide-angle X-ray scattering, we demonstrated that H atoms get progressively trapped into the Pd lattice. H trapping progressively expands the Pd lattice, leading to stabilization of the PdH_x-β lattice. The 3.6 nm Pd nanoparticles investigated in this study lost 19 % of their initial H sorption capacity during successive 50 H insertion/de-insertion cycles between 0.025 and 0.600 V at a potential sweep rate of 5 mV s^{-1}. The trapped H atoms can be desorbed by vacuum-pumping and heating to 150°C.

ASSOCIATED CONTENT

This information is available free of charge on the ACS Publications website at https://pubs.acs.org/XXXXX.

Supporting Information

Details and methods about the electrocatalyst used, electrochemical measurements, hydrogen loading quantification, *in situ* synchrotron wide-angle X-ray scattering measurements, Rietveld refinement, *in situ* ICP-MS measurements, TEM imaging.

AUTHOR INFORMATION

Corresponding Author

Frédéric Maillard − Univ. Grenoble Alpes, Univ. Savoie Mont Blanc, CNRS, Grenoble INP* (*Institute of Engineering and Management Univ. Grenoble Alpes), LEPMI, Grenoble 38000, France; https://orcid.org/0000-0002-6470-890020h; email : frederic.maillard@grenoble-inp.fr.

Authors

Arnaud Viola − Univ. Grenoble Alpes, Univ. Savoie Mont Blanc, CNRS, Grenoble INP* (*Institute of Engineering and Management Univ. Grenoble Alpes), LEPMI, Grenoble 38000, France; https://orcid.org/0000-0002-4933-3127

Raphaël Chattot − ICGM, Univ. Montpellier, CNRS, ENSCM, Montpellier 34095 Cedex 5, France; https://orcid.org/0000-0001-6169-530X; e-mail : raphael.chattot@umontpellier.fr

Galina Tisrlina − Univ. Grenoble Alpes, Univ. Savoie Mont Blanc, CNRS, Grenoble INP* (*Institute of Engineering and Management Univ. Grenoble Alpes), LEPMI, Grenoble 38000, France ; https://orcid.org/0000-0003-1587-394X; e-mail : et120659@gmail.com

Vincent Martin − Univ. Grenoble Alpes, Univ. Savoie Mont Blanc, CNRS, Grenoble INP* (*Institute of Engineering and Management Univ. Grenoble Alpes), LEPMI, Grenoble 38000, France ; https://orcid.org/orcid.org/0000-0002-9521-4137 ; e-mail : vincent.martin@grenoble-inp.fr.

Jaysen Nelayah − Université Paris Cité, CNRS, Laboratoire Matériaux et Phénomènes Quantiques, 10 rue Alice Domon et Léonie Duquet, 75013 Paris, France ; https://orcid.org/0000-0001-7349-7394; e-mail : jaysen.nelayah@u-paris.fr

Jakud Drnec − ESRF, The European Synchrotron, 71 Avenue des Martyrs, CS40220, 38043 Grenoble Cedex 9, France ; https://orcid.org/0000-0002-9520-1555; e-mail: drnec@esrf.fr

Notes

The authors declare no competing financial interest.

ACKNOWLEDGEMENTS

This project has received funding from the European Union's Horizon 2020 research and innovation program under grant agreement HERMES Nº 952184. The authors thank ESRF for the provision of the beamtime at ID31 beamline. GT is grateful to Pause program for support.

REFERENCES

(1) Dekura, S.; Kobayashi, H.; Kusada, K.; Kitagawa, H. Hydrogen in Palladium and Storage Properties of Related Nanomaterials: Size, Shape, Alloying, and Metal-Organic Framework Coating Effects. *ChemPhysChem*. Wiley-VCH Verlag May 16, 2019, pp 1158–1176. https://doi.org/10.1002/cphc.201900109.

(2) Rahimpour, M. R.; Samimi, F.; Babapoor, A.; Tohidian, T.; Mohebi, S. Palladium Membranes Applications in Reaction Systems for Hydrogen Separation and Purification: A Review. *Chem. Eng. Process. Process. Intensif.* **2017**, *121*, 24–49. https://doi.org/10.1016/j.cep.2017.07.021.

(3) Hatlevik, Ø.; Gade, S. K.; Keeling, M. K.; Thoen, P. M.; Davidson, A. P.; Way, J. D. Palladium and Palladium Alloy Membranes for Hydrogen Separation and Production: History, Fabrication Strategies, and Current Performance. *Sep. Purif. Technol.* **2010**, *73* (1), 59–64. https://doi.org/10.1016/j.seppur.2009.10.020.

(4) Behzadi Pour, G.; Fekri Aval, L.; Nasiri Sarvi, M.; Fekri Aval, S.; Nazarpour Fard, H. Hydrogen Sensors: Palladium-Based Electrode. *J. Mater. Sci.: Mater. Electron.* **2019**, *30* (9), 8145–8153. https://doi.org/10.1007/s10854-019-01190-7.

(5) Ndaya, C. C.; Javahiraly, N.; Brioude, A. Recent Advances in Palladium Nanoparticles-Based Hydrogen Sensors for Leak Detection. *Sensors* **2019**, *19* (20), 4478. https://doi.org/10.3390/s19204478.

(6) Joudeh, N.; Saragliadis, A.; Koster, G.; Mikheenko, P.; Linke, D. Synthesis Methods and Applications of Palladium Nanoparticles: A Review. *Front. Nanotechnol.* **2022**, *4*. https://doi.org/10.3389/fnano.2022.1062608.

(7) Saldan, I.; Semenyuk, Y.; Marchuk, I.; Reshetnyak, O. Chemical Synthesis and Application of Palladium Nanoparticles. *J. Mater. Sci.* **2015**, *50* (6), 2337–2354. https://doi.org/10.1007/s10853-014-8802-2.

(8) Flanagan, T. B.; Lewis, F. A. Electrode Potentials of the Palladium + Hydrogen System. *Trans. Faraday Soc.* **1959**, *55*, 1409. https://doi.org/10.1039/tf9595501409.

(9) Landers, A. T.; Peng, H.; Koshy, D. M.; Lee, S. H.; Feaster, J. T.; Lin, J. C.; Beeman, J. W.; Higgins, D.; Yano, J.; Drisdell, W. S. et al. Dynamics and Hysteresis of Hydrogen Intercalation and Deintercalation in Palladium Electrodes: A Multimodal *In Situ* X-Ray Diffraction, Coulometry, and Computational Study. *Chem. Mater.* **2021**, *33* (15), 5872–5884. https://doi.org/10.1021/acs.chemmater.1c00291.

(10) Chattot, R.; Martens, I.; Mirolo, M.; Ronovsky, M.; Russello, F.; Isern, H.; Braesch, G.; Hornberger, E.; Strasser, P.; Sibert, E. et al. Electrochemical Strain Dynamics in Noble

Metal Nanocatalysts. *J. Am. Chem. Soc.* **2021**, *143* (41), 17068–17078. https://doi.org/10.1021/jacs.1c06780.

(11) Benck, J. D.; Jackson, A.; Young, D.; Rettenwander, D.; Chiang, Y. M. Producing High Concentrations of Hydrogen in Palladium via Electrochemical Insertion from Aqueous and Solid Electrolytes. *Chem. Mater.* **2019**, *31* (11), 4234–4245. https://doi.org/10.1021/acs.chemmater.9b01243.

(12) Auer, W.; Grabke, H. J. The Kinetics of Hydrogen Absorption in Palladium (α- and β-Phase) and Palladium-Silver-Alloys. *Ber. Bunsenges. Physik. Chem.* **1974**, *78* (1), 58–67. https://doi.org/10.1002/bbpc.19740780110.

(13) Ulvestad, A.; Welland, M. J.; Cha, W.; Liu, Y.; Kim, J. W.; Harder, R.; Maxey, E.; Clark, J. N.; Highland, M. J.; You, H. et al. Three-Dimensional Imaging of Dislocation Dynamics during the Hydriding Phase Transformation. *Nat. Mater.* **2017**, *16* (5), 565–571. https://doi.org/10.1038/nmat4842.

(14) Zhang, T.; Nakagawa, Y.; Wakasugi, T.; Isobe, S.; Wang, Y.; Hashimoto, N.; Ohnuki, S. Hydrogen Absorption of Palladium Thin Films Observed by *In Situ* Transmission Electron Microscopy with an Environmental Cell. *ACS Appl. Mater. Interfaces* **2016**, *8* (23), 14548–14551. https://doi.org/10.1021/acsami.6b02971.

(15) Luo, S.; Flanagan, T. B. Supersaturation and Hydride Formation in the Dilute Phase of Pd-H and Pd-Mn-H Alloys. *J. Alloys Compd.* **2006**, *419*, 110–117. https://doi.org/10.1016/j.jallcom.2005.10.015.

(16) Flanagan, T. B.; Lynch, J. F.; Clewley, J. D.; Von Turkovich, B. The Effect of Lattice Defects on Hydrogen Solubility in Palladium. *J. Less-Common Met.* **1976**, *49*, 13–24. https://doi.org/10.1016/0022-5088(76)90022-9.

(17) Cabrera, A. L.; Erie Morales L.; Hasen, J.; Schuller, I. K. Structural Changes Induced by Hydrogen Absorption in Palladium and Palladium-Ruthenium Alloys. *Appl. Phys. Lett.* **1995**, *66*, 1216. https://doi.org/10.1063/1.113241.

(18) Krause, W.; Kahlenberg, L. On Palladium-Hydrogen. *Trans. Electrochem. Soc.* **1935**, *68* (1), 449. https://doi.org/10.1149/1.3493885.

(19) Lee, E.; Lee, J. M.; Koo, J. H.; Lee, W.; Lee, T. Hysteresis Behavior of Electrical Resistance in Pd Thin Films during the Process of Absorption and Desorption of Hydrogen Gas. *Int. J. Hydrogen Energy* **2010**, *35* (13), 6984–6991. https://doi.org/10.1016/j.ijhydene.2010.04.051.

(20) Vogel, W.; He, W.; Huang, Q. H.; Zou, Z.; Zhang, X. G.; Yang, H. Palladium Nanoparticles "Breathe" Hydrogen; a Surgical View with X-Ray Diffraction. *Int. J. Hydrogen Energy* **2010**, *35* (16), 8609–8620. https://doi.org/10.1016/j.ijhydene.2010.05.117.

(21) Bardhan, R.; Hedges, L. O.; Pint, C. L.; Javey, A.; Whitelam, S.; Urban, J. J. Uncovering the Intrinsic Size Dependence of Hydriding Phase Transformations in Nanocrystals. *Nat. Mater.* **2013**, *12* (10), 905–912. https://doi.org/10.1038/nmat3716.

(22) Nützenadel, C.; Züttel, A.; Chartouni, D.; Schmid, G.; Schlapbach, L. Critical Size and Surface Effect of the Hydrogen Interaction of Palladium Clusters. *Eur. Phys. J. D* **2000**, *8* (2), 245–250. https://doi.org/10.1007/s100530050033.

(23) Jose, D.; Jagirdar, B. R. Nature of Hydrogen Atom Trapped inside Palladium Lattice. *Int. J. Hydrogen Energy* **2010**, *35* (13), 6804–6811. https://doi.org/10.1016/j.ijhydene.2010.03.117.

(24) Sachs, C.; Pundt, A.; Kirchheim, R.; Winter, M.; Reetz, M. T.; Fritsch, D. Solubility of Hydrogen in Single-Sized Palladium Clusters. *Phys. Rev. B* **2001**, *64* (7), 075408. https://doi.org/10.1103/PhysRevB.64.075408.

(25) Pundt, A.; Sachs, C.; Winter, M.; Reetz, M. T.; Fritsch, D.; Kirchheim, R. Hydrogen Sorption in Elastically Soft Stabilized Pd-Clusters. *J. Alloys Compd.* **1999**, *293–295*, 480–483. https://doi.org/10.1016/S0925-8388(99)00469-7.

(26) Kobayashi, H.; Yamauchi, M.; Kitagawa, H.; Kubota, Y.; Kato, K.; Takata, M. On the Nature of Strong Hydrogen Atom Trapping inside Pd Nanoparticles. *J. Am. Chem. Soc.* **2008**, *130* (6), 1828–1829. https://doi.org/10.1021/ja7102372.

(27) Liu, W.; Magnin, Y.; Förster, D.; Bourgon, J.; Len, T.; Morfin, F.; Piccolo, L.; Amara, H.; Zlotea, C. Size-Dependent Hydrogen Trapping in Palladium Nanoparticles. *J. Mater. Chem. A* **2021**, *9* (16), 10354–10363. https://doi.org/10.1039/d0ta12174f.

(28) Campesi, R.; Cuevas, F.; Gadiou, R.; Leroy, E.; Hirscher, M.; Vix-Guterl, C.; Latroche, M. Hydrogen Storage Properties of Pd Nanoparticle/Carbon Template Composites. *Carbon N Y* **2008**, *46* (2), 206–214. https://doi.org/10.1016/j.carbon.2007.11.006.

(29) Rather, S.; Zacharia, R.; Hwang, S. W.; Naik, M.; Nahm, K. S. Hyperstoichiometric Hydrogen Storage in Monodispersed Palladium Nanoparticles. *Chem. Phys. Lett.* **2007**, *438* (1–3), 78–84. https://doi.org/10.1016/j.cplett.2007.02.069.

(30) Łukaszewski, M.; Czerwiński, A. The Method of Limited Volume Electrodes as a Tool for Hydrogen Electrosorption Studies in Palladium and Its Alloys. *J. Solid State Electrochem.* **2011**, *15* (11–12), 2489–2522. https://doi.org/10.1007/s10008-011-1506-5.

(31) Sherbo, R. S.; Moreno-Gonzalez, M.; Johnson, N. J. J.; Dvorak, D. J.; Fork, D. K.; Berlinguette, C. P. Accurate Coulometric Quantification of Hydrogen Absorption in Palladium Nanoparticles and Thin Films. *Chem. Mater.* **2018**, *30* (12), 3963–3970. https://doi.org/10.1021/acs.chemmater.8b01324.

(32) Paciok, P.; Schalenbach, M.; Carmo, M.; Stolten, D. On the Mobility of Carbon-Supported Platinum Nanoparticles towards Unveiling Cathode Degradation in Water Electrolysis. *J. Power Sources* **2017**, *365*, 53–60. https://doi.org/10.1016/j.jpowsour.2017.07.033.

(33) Chattot, R.; Roiron, C.; Kumar, K.; Martin, V.; Campos Roldan, C. A.; Mirolo, M.; Martens, I.; Castanheira, L.; Viola, A.; Bacabe, R. et al. Break-In Bad: On the Conditioning of Fuel Cell Nanoalloy Catalysts. *ACS Catal.* **2022**, *12*, 15675–15685. https://doi.org/10.1021/acscatal.2c04495.

(34) Abbou, S.; Chattot, R.; Martin, V.; Claudel, F.; Solà-Hernandez, L.; Beauger, C.; Dubau, L.; Maillard, F. Manipulating the Corrosion Resistance of SnO_2 Aerogels through Doping for Efficient and Durable Oxygen Evolution Reaction Electrocatalysis in Acidic Media. *ACS Catal.* **2020**, *10* (13), 7283–7294. https://doi.org/10.1021/acscatal.0c01084.

(35) Lewis, F. The Palladium-Hydrogen System: Structures near Phase Transition and Critical Points. *Int. J. Hydrogen Energy* **1995**, *20* (7), 587–592. https://doi.org/10.1016/0360-3199(94)00113-E.

(36) Bucur, R. V. Effect of Trapping on the Solubility and Diffusivity of Hydrogen in Palladium (α-Phase). *J. Mater. Sci.* **1987**, *22* (9), 3402–3406. https://doi.org/10.1007/BF01161212.

(37) Rusanova, M. Y.; Grden, M.; Czerwinski, A.; Tsirlina, G. A.; Petrii, O. A.; Safonova, T. Y. Isotope Effects in α-PdH(D) as an Instrument for Diagnosing Bulk Defects. *J. Solid State Electrochem.* **2001**, *5* (3), 212–220. https://doi.org/10.1007/s100080000135.

(38) Zhao, Z.; Huang, X.; Li, M.; Wang, G.; Lee, C.; Zhu, E.; Duan, X.; Huang, Y. Synthesis of Stable Shape-Controlled Catalytically Active β-Palladium Hydride. *J. Am. Chem. Soc.* **2015**, *137* (50), 15672–15675. https://doi.org/10.1021/jacs.5b11543.

(39) Schmidt, T. O.; Ngoipala, A.; Arevalo, R. L.; Watzele, S. A.; Lipin, R.; Kluge, R. M.; Hou, S.; Haid, R. W.; Senyshyn, A.; Gubanova, E. L. et al. Elucidation of Structure–Activity Relations in Proton Electroreduction at Pd Surfaces: Theoretical and Experimental Study. *Small* **2022**, *18* (30), 2202410. https://doi.org/10.1002/smll.202202410.

TOC Graphic

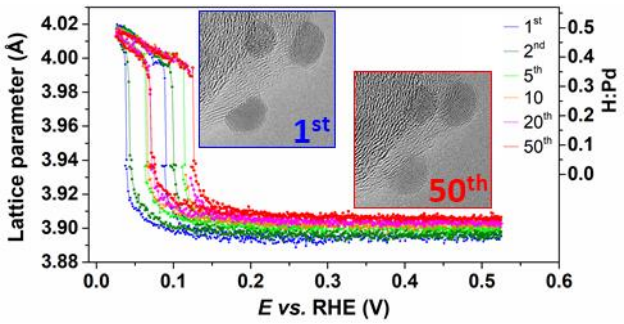

By combining *in situ* X-ray scattering and electrochemistry, we provide evidence of continuous expansion of the lattice of 3.6 nm carbon-supported Pd nanoparticles during repeated H insertion/de-insertion cycles, resulting in a progressive loss of their reversible H sorption capacity.